SOIL PARAMETERS AFFECTING PORE-PRESSURE BUILDUP DURING EARTHQUAKES

Mehmet A. Sherif[I], Isao Ishibashi[II], and Wen-Lon Cheng[III]

SUMMARY

In this paper, the authors propose equations that predict pore-pressure rise and liquefaction potential for saturated sands under earthquake-type loading. Also, the four soil parameters, C_1, C_2, C_3, and α, that are used in these equations are presented as functions of volume-decrease potential and void ratio. It should be recognized that soil shape and angularity play a role in a soil's liquefaction potential.

INTRODUCTION AND DEFINITIONS

Soil is said to have liquefied when it temporarily loses all of its load-carrying capacity. This happens when the value of the pore pressure in the soil during an earthquake reaches the magnitude of the pre-earthquake effective confining pressures σ_c' around the soil sample. To assess soil liquefaction potential, therefore, one must be able to predict the pore-pressure buildup in the soil mass under earthquake loading.

Based on their extensive investigation on Ottawa sands, the authors have proposed Eqs. 1 and 2 (Ishibashi et al., 1977; Sherif et al., 1978) for the prediction of pore-pressrue rise in saturated sands under uniform and non-uniform dynamic loadings.

Under uniform loading:

$$\Delta U_N^* = (1 - U_{N-1}^*) \frac{C_1 N}{N^{C_2} - C_3} \cdot \left(\frac{\tau_N}{\sigma'_{N-1}}\right)^{\alpha} \tag{1}$$

Under non-uniform loading:

$$\Delta U_N^* = (1 - U_{N-1}^*) \frac{C_1 N_{eq}}{N_{eq}^{C_2} - C_3} \cdot \left(\frac{\tau_N}{\sigma'_{N-1}}\right)^{\alpha} \tag{2}$$

where ΔU_N^* is the normalized (pore pressure over initial confining pressure) incremental pore-pressure rise during the N^{th} cycle; U_{N-1}^* is the total normalized pore-pressure value at the end of the $N\text{-}1^{th}$ cycle; τ_N is the applied earthquake shear stress at the N^{th} cycle; σ'_{N-1} is the effective confining pressure at the end of the $N\text{-}1^{th}$ cycle; C_1, C_2, C_3, and α are soil parameters; N is the number of uniform stress cycles; and N_{eq} is the

---

I Professor of Civil Engineering and Adjunct Professor of Quaternary Research, University of Washington, Seattle, U.S.A.

II Research Associate Professor of Civil Engineering, University of Washington

III Graduate Student in Civil Engineering, University of Washington

equivalent number of uniform stress cycles determined from non-uniform loading and is defined as

$$N_{eq} = \sum_{i=1}^{N} \left(\frac{\tau_i}{\tau_N} \right)^{\alpha} \tag{3}$$

where τ_i is the shear stress at the i^{th} non-uniform loading cycle.

In this paper, uniform loading is defined as one where the peak positive stresses τ_p (above zero crossing) and peak negative stresses τ_n (below zero crossing) are equal at all times (see Fig. 1). Non-uniform loading is defined as one where τ_p equals τ_n within each stress cycle. Earthquake loading is defined as one where no restrictions whatsoever are imposed. Also, each zero crossing of the stress/time diagram is taken as half a cycle. In their earlier studies on loose Ottawa sand, the authors found excellent correlation between the pore pressures predicted by Eqs. 1 and 2 and those found experimentally in laboratory tests conducted under both uniform and non-uniform loadings. In this paper the previous findings on pore-pressure prediction under uniform and non-uniform loading are extended to the prediction of pore-pressure rise under earthquake-type loadings. Furthermore, data is provided from which the four soil parameters, C_1, C_2, C_3, and α, used in the pore-pressure-prediction equations can be obtained.

PORE-PRESSURE RISE UNDER EARTHQUAKE LOADINGS

Eq. 2, which predicts pore-pressure rise in a saturated soil under non-uniform dynamic loading, can also be made to apply to the prediction of pore-pressure rise under earthquake loading, provided that the random stress variation during the earthquake stress/time history is represented by an equivalent number of uniform stress cycles. In order to do this, reference is made to Fig. 2. Let us assume that Fig. 2(a) represents any arbitrary N^{th} earthquake stress cycle in which the positive stress τ_{Np} does not equal τ_{Nn}. The random positive and negative stress variation in Fig. 2(a) can be represented by two fictitious full-cycle uniform stresses, one corresponding to the positive stress τ_{Np} and the other to the negative stress τ_{Nn}, as shown in Figs. 2(b) and 2(c) respectively. In view of the fact that the values of both the positive and negative shear stresses τ_{Np} and τ_{Nn} are doubled through this process, the values of the incremental pore pressures generated under the stresses shown in Figs. 2(b) and 2(c) should therefore equal twice the incremental pressure rise under the actual earthquake stress cycle shown in Fig. 2(a). Accordingly,

$$\Delta U_N^* = \frac{1}{2} \left(\Delta U_{Np}^* + \Delta U_{Nn}^* \right) \tag{4}$$

Considering the above relationship, the value of the total normalized pore pressure at the end of the N^{th} earthquake cycle will therefore be

$$U_N^* = U_{N-1}^* + \frac{1}{2} \left(\Delta U_{Np}^* + \Delta U_{Nn}^* \right) \tag{5}$$

When the value of the normalized total pore pressure U_N^* in Eq. 5 reaches unity (one), then the soil will reach liquefaction stage.

In view of the fact that the actual earthquake stress cycle in Fig. 2(a) has been separated into two uniform positive and negative stress cycles, it is necessary therefore that the individual effects of the positive and negative stress components be likewise considered separately, together with their associated pore pressures and equivalent numbers of stress cycles.

Therefore, the magnitudes of ΔU_{Np}^*, ΔU_{Nn}^*, $(N_{eq})_p$, and $(N_{eq})_n$ can be calculated from the expressions outlined in Eqs. 6, 7, 8, and 9 respectively.

$$\Delta U_{Np}^* = (1 - U_{N-1}^*) \cdot \frac{C_1 (N_{eq})_p}{(N_{eq})_p^{C_2} - C_3} \cdot \left(\frac{\tau_{Np}}{\sigma'_{N-1}} \right)^{\alpha} \tag{6}$$

$$\Delta U_{Nn}^* = (1 - U_{N-1}^*) \cdot \frac{C_1 (N_{eq})_n}{(N_{eq})_n^{C_2} - C_3} \cdot \left(\frac{\tau_{Nn}}{\sigma'_{N-1}} \right)^{\alpha} \tag{7}$$

$$(N_{eq})_p = \sum_{i=1}^{N} \left(\frac{\tau_{ip}}{\tau_{Np}} \right)^{\alpha} \tag{8}$$

$$(N_{eq})_n = \sum_{i=1}^{N} \left(\frac{\tau_{in}}{\tau_{Nn}} \right)^{\alpha} \tag{9}$$

where τ_{Np} and τ_{Nn} are the maximum positive and negative stresses at the N^{th} cycle at which the normalized pore-pressure value is to be calculated; τ_{ip} and τ_{in} are the maximum positive and negative shear stresses at the i^{th} cycle; ΔU_{Np}^* and ΔU_{Nn}^* are the normalized incremental pore pressures due to actual earthquake-induced positive and negative shear stresses τ_{Np} and τ_{Nn} respectively; and $(N_{eq})_p$ and $(N_{eq})_n$ are the equivalent number of positive and negative random earthquake stress cycles.

Since the wide applicability and general practical use of Eqs. 5 through 9 will be greatly dependent on the ease with which the soil parameters C_1, C_2, C_3, and α are obtained, an extensive series of laboratory experiments was undertaken for that purpose, and the data obtained from these tests are shown in Figs. 3, 4, and 5. Soils tested in connection with determination of the above soil parameters were prepared in the laboratory so that they had the same coefficient of uniformity and mean diameter but different angularity. Figs. 3 and 4 respectively show that the values of C_1 and α are functions of volume-decrease potential $(e - e_{min})$, except that the C_1 parameter also depends on soil type, while the α values are only a function of volume-decrease potential irrespective of soil type. Furthermore, it is interesting to note that the soil parameters C_2 and C_3 are nearly constant and are nearly equal to 2 and 0.5 for all sands

irrespective of their void ratio or density.

Fig. 6 shows a comparison of the pore-pressure buildup predicted by using Eqs. 5 through 9 with that measured experimentally in the laboratory under the earthquake shear stresses shown in this figure. It is evident from Fig. 6 that these equations do indeed provide an adequate base for the prediction of pore-pressure rise in saturated sands under earthquake-type loading.

The above new pore-pressure-rise prediction Eqs. 5 through 9 were used to predict the liquefaction potential of a 2-ft.-thick saturated sand deposit shown in Fig. 7, under the earthquake stresses shown in Fig. 8(a). By inserting the soil parameter values shown in Fig. 7 ($C_1 = 2.4$, $C_2 = 1.8$, $C_3 = 0.3$, $\alpha = 2.17$) and the pre-earthquake effective confining soil pressure $\sigma_m' = 5.31$ psi into the above equations, it is found that the above soil deposit will liquefy during the eighth cycle, which occurs 5 seconds from the start of the earthquake, as shown by Curve A in Fig. 8.

In order to illustrate the effects of the confining pressures on soil liquefaction, it was decided to investigate the liquefaction potential of the same soil deposit shown in Fig. 7 under the same earthquake stresses in Fig. 8(b), assuming that soil element A in Fig. 7 is at a depth of 33 ft. from the ground surface, where the mean confining pressure around it would have been about 20 psi instead of 5.31 psi. As shown by Curve B in Fig. 8, the maximum value of the normalized pore pressure U_N^* under these new circumstances would have been equal to 0.54 at the end of the earthquake, thus suggesting that if the soil were located at a depth of 33 ft. from the ground surface it would not have liquefied under the same earthquake stresses.

To investigate the effects of soil density on its liquefaction potential, an earthquake stress signal shown in Fig. 9(a) was applied on loose, medium dense, and dense saturated Ottawa sands and the values of the normalized pore pressures predicted by Eqs. 5 through 9 were recorded as shown in Fig. 9(b). It can be observed from this figure that the loose soil deposit liquefies after 5 seconds, while the same soil deposit with medium density liquefies after 10 seconds. On the other hand, if the above soil were dense it would not liquefy at all during this particular earthquake. It is also evident from Fig. 9 that it is mainly the large peak shear stresses that contribute significantly to pore-pressure rise.

REFERENCES

Ishibashi, I., M. A. Sherif and C. Tsuchiya (1977), "Pore-Pressure Rise Mechanism and Soil Liquefaction," Soils and Foundations, Jap. Soc. of Soil Mech. and Found. Engrg., V.17, No.2, pp.17-27.

Sherif, M. A., I. Ishibashi and C. Tsuchiya (1978), "Pore-Pressure Prediction during Earthquake Loadings," Soils and Foundations, Jap. Soc. of Soil Mech. & Found. Engrg., V.18, No.4, pp.19-30.

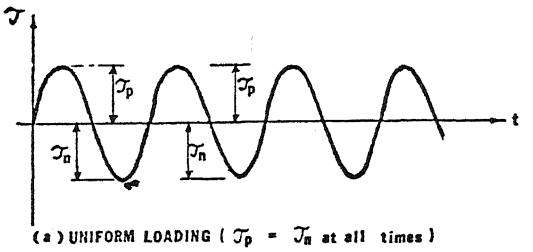

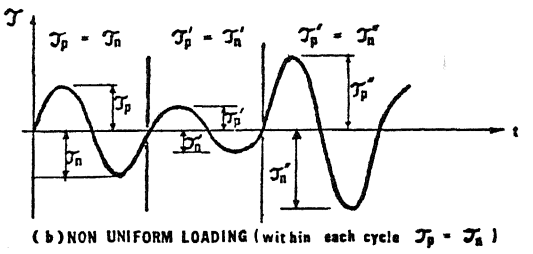

Fig. 1. Types of loadings.

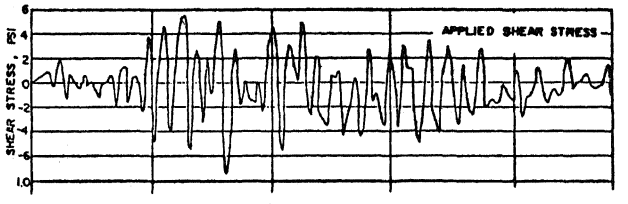

(c) EARTHQUAKE LOADING (no restrictions)

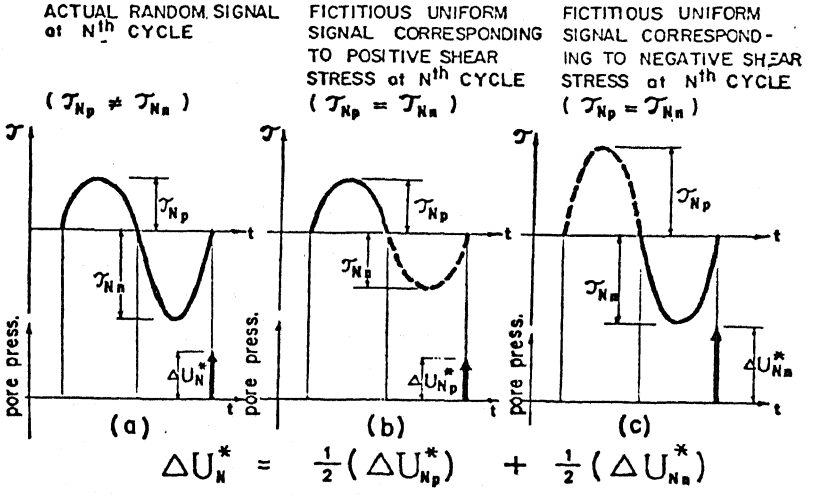

Fig. 2. Pore-pressure rise under random signal.

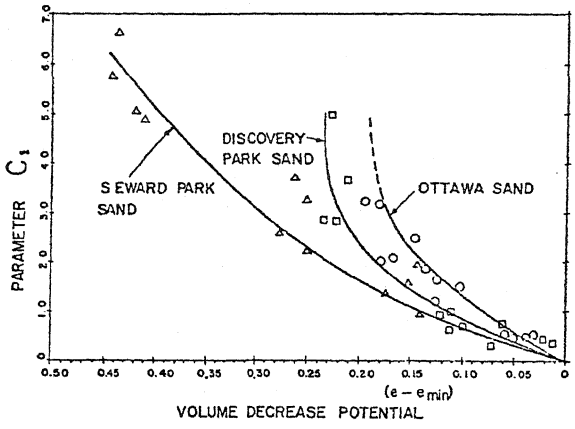

Fig. 3. Relationship between Parameter C_1 and volume decrease potential.

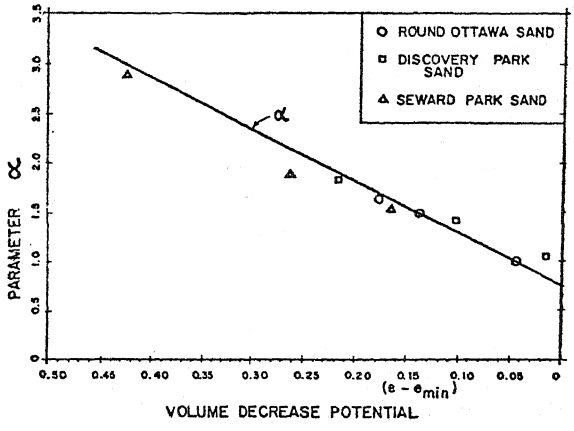

Fig. 4. Relationship between Parameter α and volume decrease potential.

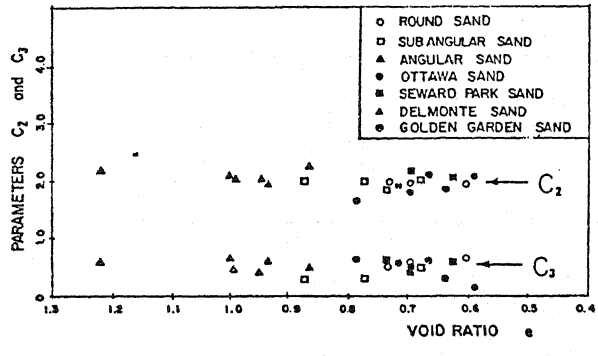

Fig. 5. Relationships between Parameters C_2 and C_3 and void ratio.

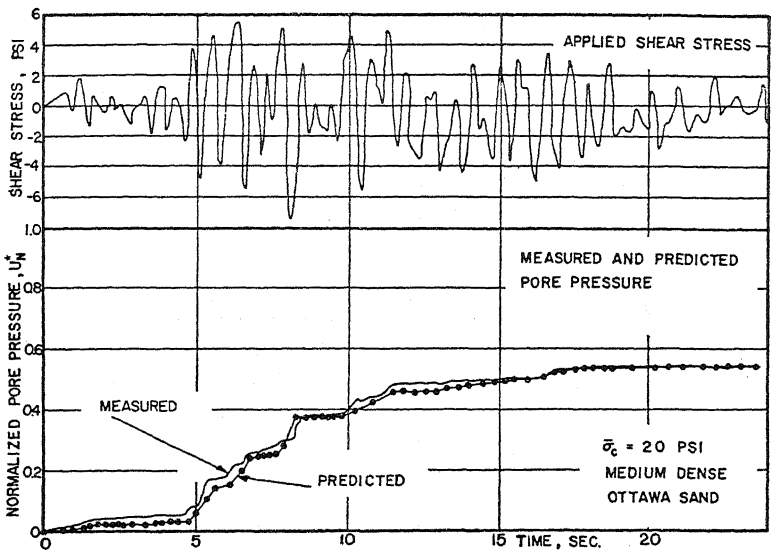

Fig. 6. Pore-pressure rise under earthquake-type loading.

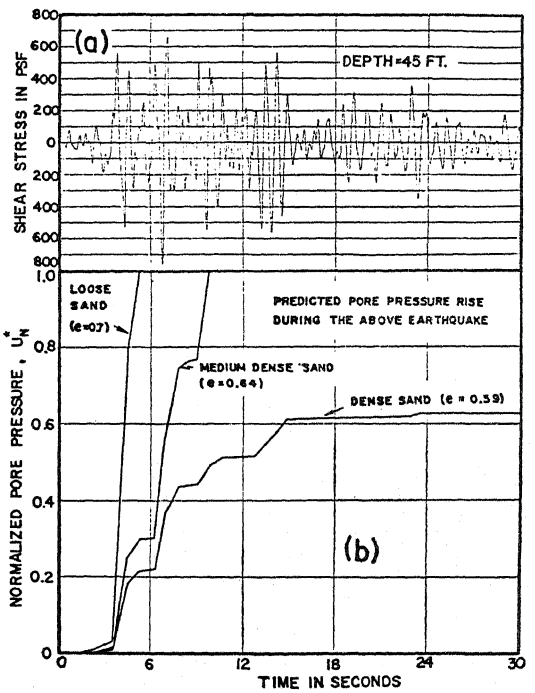

Fig. 9. Predicted pore-pressure rise during earthquake.

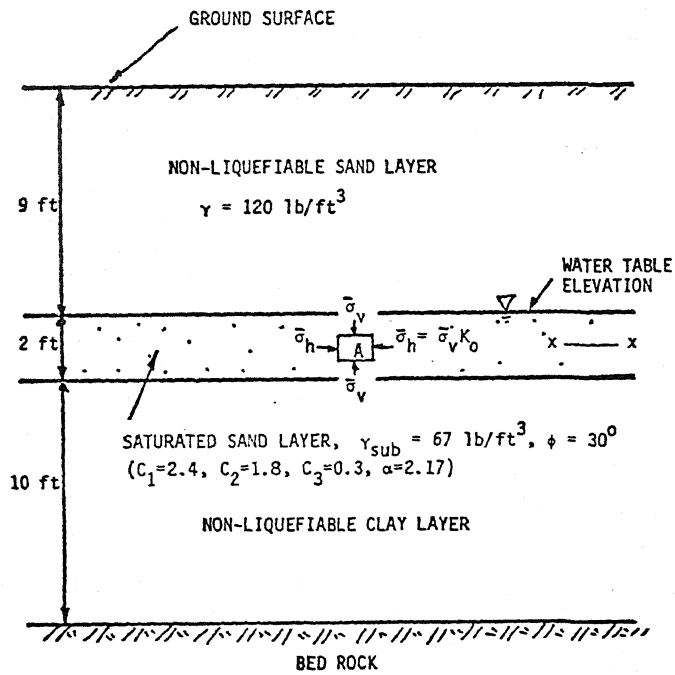

Fig. 7. Illustrative problem.

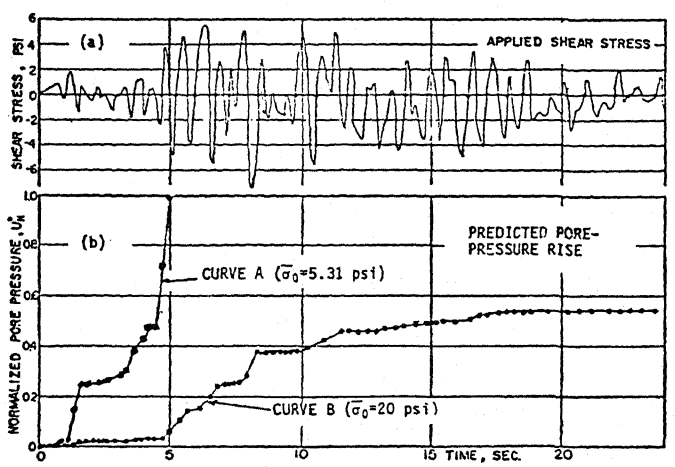

Fig. 8. Prediction of soil liquefaction potential as a function of earthquake stresses and confining pressures.